Nanoscale

MINIREVIEW

View Article Online
View Journal | View Issue

Cite this: *Nanoscale*, 2022, **14**, 3398

Support effects of metal–organic frameworks in heterogeneous catalysis

Masaaki Sadakiyo

Catalytic support effects have been widely studied as a key factor for creating highly active heterogeneous catalysts with limited amounts of rare metal elements. Recently, support effects of metal–organic frameworks (MOFs) started to be investigated using their wide variety in pore size, electronic state, and selective adsorption property. Three types of support effects, namely molecular sieving, charge transfer, and substrate adsorption effects, have been reported on composite catalysts of metal nanoparticles supported on MOFs (M/MOFs). The current reports on heterogeneous catalysis in M/MOFs clearly demonstrated that both catalytic activity and product selectivity can be drastically enhanced and modulated by MOF supports through these support effects, and that application of MOFs as the supports is beneficial for creating novel high performance catalysts with metal nanoparticles. This minireview summarizes the catalytic properties and support effects observed on M/MOFs.

Received 20th November 2021,
Accepted 14th February 2022

DOI: 10.1039/d1nr07659k

rsc.li/nanoscale

1. Introduction

Metal–organic frameworks (MOFs) have emerged as a new class of crystalline porous materials; because of their unique features such as high materials variety and designable pores, they are considered for use in various applications such as separation,[1,2] storage,[3,4] delivery,[5,6] and electrolytes.[7–9] MOFs are organic–inorganic hybrid materials and thus have both organic and inorganic characters. For example, MOFs show a relatively high thermal stability (<500 °C)[10,11] compared with pure crystalline organics that often decompose or sublimate below 200 °C,[12,13] and this is one of the inorganic characteristics of MOFs due to their strongly bound organic components through metal–ligand bonds. By contrast, MOFs can be easily modified with some functional groups by using various functionalized ligands[14] or through post-synthetic chemical reactions,[15] allowing tuning of the electronic state or porous characters of the MOFs, which is one of the organic characteristics of the MOFs. Because of the relatively high thermal stability and designable architectures together with the high porosity, there has been a strong expectation for MOFs to be applied as new catalytic support materials for heterogeneous catalysis.[16,17]

Catalytic support is one of the critical components of heterogeneous catalysts because of their important roles in improving the performance of catalysts. The main role of the catalytic support is to prevent aggregation of small-sized metal nanoparticles (NPs) including catalytically active sites on their surface, which allow the catalysts to show high activity for a prolonged time. Another important role is to improve the catalytic activity through the "support effects" of the support materials.[18] Support effects are some of the most important ways to create high-performance catalysts using limited amounts of rare elements such as noble metals (*e.g.* Pt). In the traditional support materials such as metal oxides, the support effects have been widely studied using metal catalysts deposited on them.[19–24] Recently, non-traditional support materials have been applied as catalytic supports to overcome the catalytic performance of traditional catalysts.[25–27] Many researchers have tried to apply MOFs as catalytic support to enhance the catalytic performance using metal–MOF compo-

Department of Applied Chemistry, Faculty of Science Division I, Tokyo University of Science, 1-3 Kagurazaka, Shinjuku-ku, Tokyo 162-8601, Japan

Masaaki Sadakiyo

*Dr Masaaki Sadakiyo is a Junior Associate Professor at Department of Applied Chemistry, Faculty of Science Division I, Tokyo University of Science. He received his Ph.D. from Kyoto University in 2012. He became an Assistant Professor at Kyushu University in 2012. He moved to Tokyo University of Science in 2019. His research interests include functionalities of metal–organic frameworks and related porous materials (*e.g. *ionic conduction, catalysis).*

sites (M/MOFs). However, the catalytic support effects of MOFs have not been well clarified compared with traditional supports and this has become a current topic in recent years.

Recent progress in preparation methods for M/MOF catalysts having intended structures allows us to know how the MOF supports exactly affect to the catalytic property of M/MOFs. Recent reports on M/MOF catalysts clearly demonstrated that MOFs truly show three types of support effects, namely molecular sieving, charge transfer, and substrate adsorption effects, which have been observed in traditional oxide-based catalysts. There are non-negligible number of well-designed M/MOF catalysts that overcome the traditional catalysts by using these support effects especially in the reactions at relatively low temperature region (<300 °C).

In this review, we summarize recent studies on the support effects of MOFs in heterogeneous catalysis. First, we briefly describe recent advances in preparation methods for M/MOFs, which are strongly related to the clarification of the support effects of MOFs. Second, we present a classification of the support effects and give examples of each support effect observed in M/MOFs.

2. Preparation of M/MOFs

Considering that many important factors modulate the catalytic activity of metal-supported catalysts, such as particle size, loading amount, and the interaction between metal and support material, an ideal way to clarify the support effects is to compare catalytic activity among catalysts having different support materials with similar other factors (*i.e.* size, loading amount, direct contact with the support). However, for M/MOF catalysts, there are few rational methods of preparing such ideal samples because the general preparation method for oxide-based catalysts, such as impregnation with calcination at high temperature, cannot be widely applied for MOFs because of their moderate thermal stability (<500 °C). Therefore, to clarify the catalytic support effects of MOFs, the preparation method is of importance. This section summarizes recent advances and the most common preparation methods for M/MOFs.

Previously, M/MOFs have been synthesized through various methods such as solution impregnation,[28,29] chemical vapour deposition,[30,31] and solid grinding,[32,33] followed by a chemical reduction process. These methods are similar to some methods used for other metal-loaded catalysts. By contrast, some other processes have been developed as specific methods for M/MOFs. Lu *et al.* reported an encapsulation method that consists of the incorporation of polymer-coated NPs inside MOFs during the crystallization process of the MOFs (Fig. 1).[34] Preliminarily-synthesized NPs, such as Ag, Au, Pt, Fe_3O_4, $NaYF_4$, and CdTe, which are coated with poly(*N*-vinylpyrrolidone) (PVP) as a protecting reagent, were incorporated in ZIF-8. The framework of ZIF-8 is formed at room temperature (RT) and thus the NPs can be incorporated inside the ZIF-8 crystals at RT through the high affinity between ZIF-8 and PVP. Zhou *et al.* reported another encapsulation method

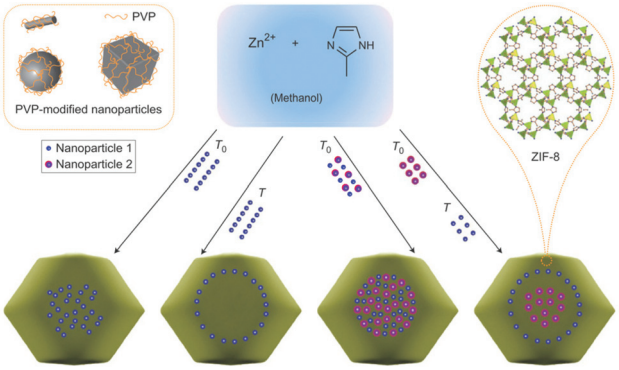

Fig. 1 Schematic illustration of the encapsulation method for M/MOFs' preparation. This figure has been reproduced from ref. 34 with permission from the Nature publishing group, copyright 2012.

using polydopamine (PDA).[35] Crystals of ZIF-8 and UiO-66 were successfully grown around PDA-coated NPs. Similar to the case with PVP, the interaction between MOF and PDA is useful for preparing the core–shell-type structure of M/MOFs. Various NPs such as Au NPs and magnetic iron oxide were encapsulated in ZIF-8 and UiO-66. In the case of UiO-66, the reaction temperature for the encapsulation was 100 °C, which is different from ZIF-8 (RT).

Mukoyoshi *et al.* reported another unique preparation method for M/MOFs, which is the partial decomposition of MOFs (Fig. 2).[36] In this method, NPs are formed inside the MOF crystals during the thermal decomposition of the MOFs. The metal sources provided by the MOF are automatically reduced by decomposition of the ligands. Ni-MOF-74, which is composed of a central metal, Ni^{2+}, and a reductive ligand, 2,5-dioxido-1,4-benzenedicarboxylate, was heated above 300 °C under vacuum to form Ni NPs in Ni-MOF-74 (Ni/Ni-MOF-74).

For the use of M/MOFs for clarification of the support effects of MOFs in heterogeneous catalysis, these methods seem not to be ideal but have some problems. For instance, in wet chemistry such as solution impregnation with a chemical reduction process, only the MOFs that are highly stable against reagents can be applied. In addition, a synthetic recipe depends on the applied MOFs and thus similar-sized NPs have difficulty forming on different supports. In the encapsulation method, the size of the metal NPs can be easily changed because it is determined in the preliminary synthesis of the NPs. However, number of applicable MOF was limited (*e.g.*

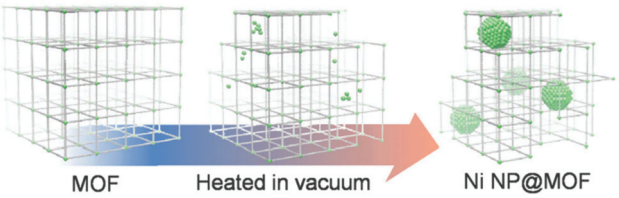

Fig. 2 Schematic illustration of the preparation of M/MOF composites through a partial decomposition method.

ZIF-8). In addition, this method requires protecting reagents that would prevent direct contact or strong interaction between the metallic NPs and the MOF support. In the partial decomposition method, the metal source is only from the MOF support and thus it is difficult to change the MOF support without changing the metal NPs.

Sadakiyo *et al.* recently reported the arc plasma deposition (APD) method that satisfies the conditions for the clarification of MOF support effects, *i.e.* similar-sized NPs, easy-to-change MOF supports, and direct contact between the NP and the MOF, at a higher level than in other methods (Fig. 3).[37] In this method, metal atoms are deposited on support materials from a metal target in a vacuum chamber. Well-dispersed similar-sized metal NPs (approximately less than 2 nm in diameter at a low-loading amount such as below 1 wt%) are formed on the surface of any MOF crystals with direct contact between the NP and the MOF. This method does not require any chemicals, solvents, and protecting reagents, in contrast to other methods. Importantly, in this method, the well-dispersed metal NPs can be loaded on different MOFs using the same technique, which would be preferable for clarifying the support effects through a systematic comparison using different MOF supports.

3. Support effects of MOFs in heterogeneous catalysis

The support effects in heterogeneous catalysis can be roughly classified into three types (Fig. 4). First is the molecular sieving effect that prevents a non-target substrate from reaching an active site of the catalysts.[19] Second is the charge-transfer effect that is caused by electronic interaction between the metal NP and the support material, resulting in modulation of the catalytic activity of the supported metal catalysts.[20] Third is the substrate adsorption effect that is caused by the strong adsorption of the substrate by the support material. If the reaction includes multiple substrates, strong adsorption for one of the substrates could help to proceed the reaction.[23] These support effects have been well investigated in traditional support materials such as oxide-based catalysts.[19–24] Considering that MOFs have tuneable pore sizes, various electronic states, and various interactions with guest molecules, they should have a strong potential to show all types of these support effects (Fig. 4). Recent progress and examples of each support effect of MOFs are described here.

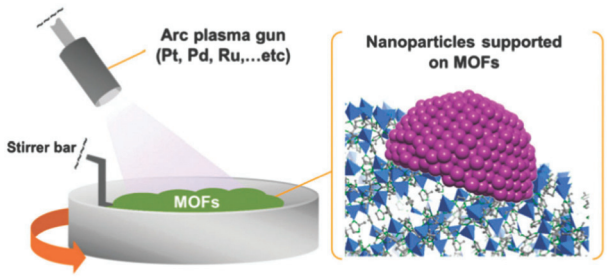

Fig. 3 Schematic illustration of the preparation of M/MOFs through the arc plasma deposition method.

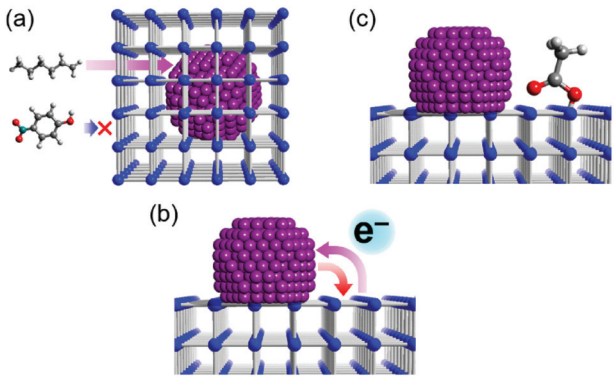

Fig. 4 Schematic illustrations of support effects in heterogeneous catalysis, regarding (a) molecular sieving, (b) charge transfer, and (c) substrate adsorption, which are illustrated with porous MOFs as the support materials.

3.1 Molecular sieving effect in M/MOFs

Because MOFs have a variety of porous structures, there is no doubt that M/MOF catalysts in which metal NPs are surrounded by MOFs show the molecular sieving effect. The encapsulation method described above is one of the most ideal methods to show the molecular sieving effect because the metal NPs are completely incorporated inside the MOF crystals. Lu *et al.* reported the molecular sieving effect in Pt NPs encapsulated by ZIF-8 (Pt/ZIF-8).[34] They showed the difference in catalytic activity for hydrogenation reaction of *n*-hexene and *cis*-cyclooctene on Pt NPs among various Pt-loaded catalysts such as Pt/CNT (CNT: carbon nanotube), T-Pt@ZIF-8 (Pt-loaded catalysts prepared by the templating method, *i.e.* solution impregnation followed by chemical reduction), and Pt/ZIF-8. ZIF-8 itself did not show any catalytic activity because the active site is located only on the Pt NPs in this reaction (Fig. 5), Pt/CNT showed catalytic activity for both

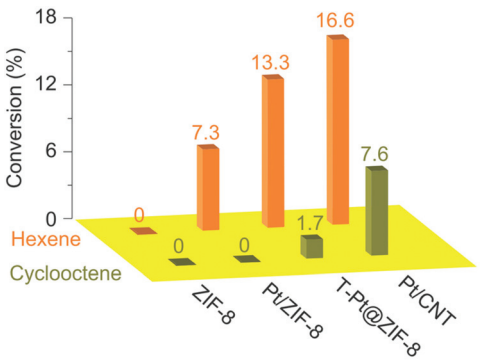

Fig. 5 Catalytic activity for the hydrogenation of *n*-hexene and *cis*-cyclooctene. This figure has been reproduced from ref. 34 with permission from the Nature publishing group, copyright 2012.

n-hexene and *cis*-cyclooctene. However, Pt/ZIF-8 showed almost no catalytic activity for *cis*-cyclooctene but showed activity for *n*-hexene, indicating that ZIF-8 acts as a molecular sieve selecting the substrates before they reach a catalytically active site on Pt NPs. Similarly, T-Pt@ZIF-8 showed a large difference in the catalytic activity for these substrates; however, the activity for *cis*-cyclooctene is not zero, which is indicative that T-Pt/ZIF-8 includes some of the Pt NPs completely exposed to the outside and that the encapsulation method is advantageous from the viewpoint of complete incorporation of the metallic NPs inside MOF crystals. Wang *et al.* also demonstrated the molecular sieving effect of ZIF-8 using the same reaction without protecting reagents for NP formation.[38] These examples clearly demonstrate that the small window size of ZIF-8 is effective for preventing the migration of large molecules such as cyclic molecules.

Guo *et al.* also reported the molecular sieving effect of Pt NPs confined in UiO-66-NH_2 crystals (Pt@UiO-66-NH_2).[39] They showed the catalytic activity of Pt@UiO-66-NH_2 for hydrogenation reactions with ethylene, 1-hexene, and cyclooctadiene (COD). The Pt@UiO-66-NH_2 catalyst showed high catalytic activity for ethylene and 1-hexene, which is similar to Pt/SiO_2 control catalyst. However, in the case of the bulky substrate of COD, the activity on Pt@UiO-66-NH_2 was drastically lower than on Pt/SiO_2 because of the limited pore size of UiO-66-NH_2 (~6 Å), which is smaller than the molecular size of the COD substrate (6.7 × 6.2 × 4.2 $Å^3$).

Zhou *et al.* reported a clear molecular sieving effect using Au NPs encapsulated in ZIF-8 and UiO-66.[40] The Au NPs were first embedded on PDA-coated magnetic iron oxide NPs (MagNP@PDA@AuNPs) and then the composite NPs, MagNP@PDA@AuNPs, were encapsulated in ZIF-8 (MagNP@PDA@AuNPs@ZIF-8) and UiO-66 (MagNP@PDA@AuNPs@UiO-66). These catalysts were applied to reduction reactions of 4-nitrophenol and methylene blue (Fig. 6). An apparent catalytic activity was observed for 4-nitrophenol on MagNP@PDA@AuNPs@UiO-66, whereas no such activity was observed on MagNP@PDA@AuNPs@ZIF-8. This indicates that the 4-nitrophenol cannot migrate in ZIF-8 but can freely pass through UiO-66 due to the larger pore size of UiO-66. By contrast, the catalytic activity for methylene blue, which is bulkier than 4-nitrophenol, was not observed even on MagNP@PDA@AuNPs@UiO-66, indicating the effective exclusion of the substrate by the surrounding MOFs around the Au NPs.

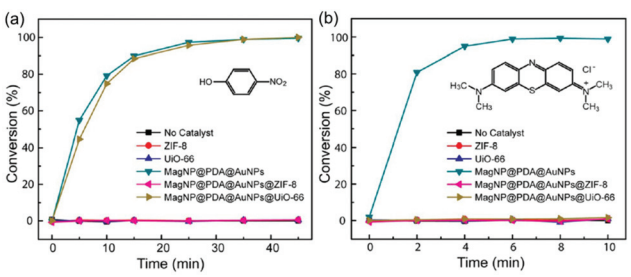

Fig. 6 Catalytic activity for (a) 4-nitrophenol and (b) methylene blue reduction reactions. This figure has been reproduced from ref 40 with permission from the American Chemical Society, copyright 2015.

3.2 Charge transfer effect in M/MOFs

The various architectures of MOFs should provide a large variety of electronic structures. In particular, the organic components included as ligands allow tuning of the electronic states of MOFs, whereas the electronic states of oxide materials are normally difficult to widely tune. As described above, the electronic interaction between a metal NP and the support is one of the dominant factors in modulating catalytic activity on the metal NP, thus the support effect regarding the charge transfer in M/MOFs is also of interest in creating highly active catalysts.

Li *et al.* reported on the difference in the catalytic activity of Pd NPs formed in UiO-66 frameworks having different functional groups (Pd@UiO-66-X; X = NH_2, OMe, H).[41] They applied Pd@UiO-66-X for the aerobic reaction between benzaldehyde and ethylene glycol. The possible products of this reaction are hemiacetal and ester (Fig. 7). The sample of X = NH_2 showed low selectivity for ester, whereas both samples of X = OMe and X = H showed high selectivity for ester. The difference in oxidation capability between these catalysts was expected to be due to the difference in the electronic states of the included Pd NPs, which were modulated by the coordination by the functional groups on MOFs: Coordination of NH_2 group to Pd NP seems to make an electron-rich surface of Pd NP. The difference in electronic states of the Pd NPs was investigated by diffuse reflectance infrared Fourier transform spectroscopy (DRIFTS) and calculation with density functional

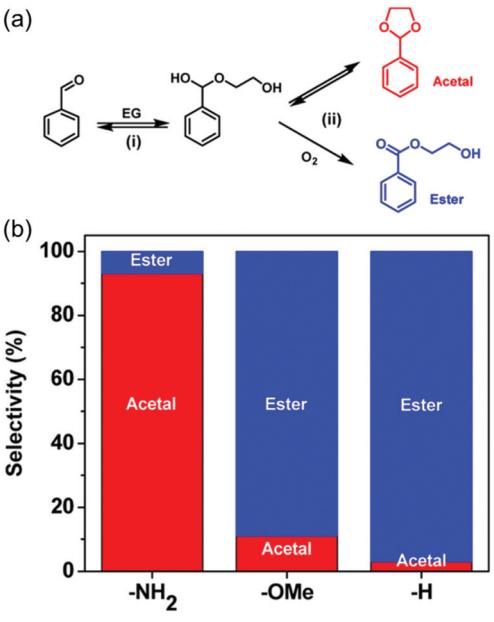

Fig. 7 (a) Scheme of the aerobic reaction between benzaldehyde and ethylene glycol (EG). (b) Product selectivity on Pd@UiO-66-X (X = NH_2, OMe, and H). This figure has been reproduced from ref. 41 with permission from the American Chemical Society, copyright 2016.

theory (DFT). In the DRIFTS measurements under CO, the vibration peak of linearly adsorbed CO molecules at around 2020–2075 cm^{-1} in Pd@UiO-66-NH_2 were observed at a lower wavenumber (2059 cm^{-1}) than in Pd@UiO-66-OMe (2071 cm^{-1}) and Pd@UiO-66 (2073 cm^{-1}). This is indicative that Pd NPs in Pd@UiO-66-NH_2 would show a stronger π back-donation to the CO due to the electron-rich surface. The DFT calculation revealed that d-band centres of Pd NPs were modulated by the coordination from the functional groups on the frameworks and that the Pd NP coordinated by the –NH_2 group would give a higher level of d-band centres compared with that coordinated by the –OMe group, which led to a higher oxidation capability of the electron-poor surface of Pd@UiO-66-OMe to give a higher selectivity for ester.

Yoshimaru *et al.* performed a systematic study on the catalytic support effect regarding charge transfer.[42] They showed a difference in the catalytic activity for the CO oxidation reaction on Pt NPs supported on different MOFs. As mentioned, there are various parameters for determining catalytic activity (*e.g.* size of the metal NPs). Therefore, to clarify the support effect, parameters other than the support material should preferably be almost the same. They prepared Pt/MOF catalysts including similar-sized Pt NPs, supported on different MOFs, with similar Pt content in the same preparation process by the APD method. Four MOFs, Zn-MOF-74, Mg-MOF-74, HKUST-1, and UiO-66-NH_2, having different electronic states, were used as support materials. Ionization potentials that directly correspond to the top level of the valence band, *i.e.* electron-donating character, were evaluated using ultraviolet photoelectron spectroscopy measurements to identify the electronic character of these MOFs. The results showed that the order of electron-donating ability would be Zn-MOF-74 (ionization potential = 5.2 eV) > Mg-MOF-74 (5.7 eV) > HKUST-1 (6.0 eV) > UiO-66-NH_2 (6.7 eV). The electronic states of the supported Pt NPs were also estimated using X-ray photoelectron spectroscopy (XPS) measurements. The binding energy (Pt^0 $4f_{7/2}$) of the Pt NPs completely depends on the MOFs and their order depends on the electron-donating character of the MOFs (Fig. 8), indicating the apparent charge-transfer interaction between the Pt NP and the MOF, *i.e.* electron donation from the MOF to the Pt NP or electron withdrawal from the Pt NP by the MOF.

The catalytic support effects were demonstrated through the difference in catalytic activity for the CO oxidation reaction, which is known to be sensitive to the NP electronic state.[43] The relationship between catalytic activity for CO oxidation (defined by T_{50}, *i.e.* the temperature at 50% conversion of CO) and the electronic state of Pt NPs supported on different MOFs (*i.e.* the binding energy of Pt (Pt^0 $4f_{7/2}$)) is shown in Fig. 9. There is a clear relationship between catalytic activity and the electronic state of the Pt NPs and that the electron-rich surface of Pt NPs (*i.e.* Pt NPs on Zn-MOF-74) is preferable for the reaction. Considering that the order of electronic states and catalytic activity is the same as that of the electron-donating ability of the MOF supports, whereas the other factors (*e.g.* Pt NPs, synthetic procedure, Pt NPs amounts) are almost the same, the catalytic activity is truly controlled by the support materials through the charge-transfer interaction between Pt NP and MOF. They also compared the turnover frequency (TOF) of the catalysts, calculated by the number of active sites estimated through chemisorption of H_2. The order of TOF at each temperature was also the same as that of electronic states of the Pt NPs, meaning that the catalytic activity of each active site on Pt NPs is modulated by the charge transfer with the MOFs.

Kobayashi *et al.* reported a charge transfer interaction between Cu and MOF, which relates to catalytic activity for methanol production through CO_2 hydrogenation reaction.[44] Cu NPs were prepared on various supports, γ-Al_2O_3, ZIF-8, MIL-100, and a series of UiO-66 based frameworks (UiO-66-X (X = H, COOH, NH_2) and Hf-UiO-66). The charge transfer between Cu NP and support was evaluated through XPS measurements. Although the shift of XPS peaks of Cu NPs (Cu 2p) was not obvious, apparent shifts of the peaks of metal components included in the support materials (*e.g.* Zr 3d peak in UiO-66) were observed in Cu/UiO-66-X and Cu/Hf-UiO-66,

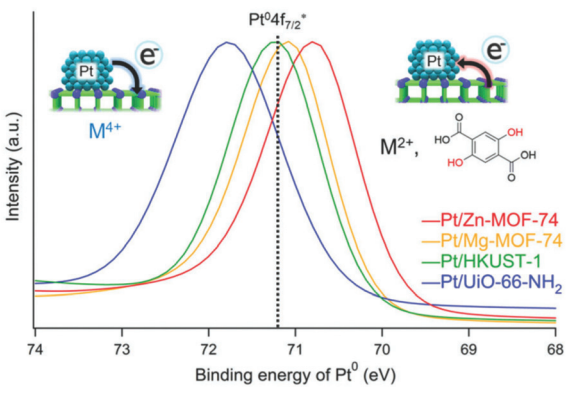

Fig. 8 Fitted curves (Pt^0 $4f_{7/2}$) of XPS spectra of (red) Pt/Zn-MOF-74, (yellow) Pt/Mg-MOF-74, (green) Pt/HKUST-1, and (blue) Pt/UiO-66-NH_2. The black dotted line indicates the binding energy of bulk Pt^0 $4f_{7/2}$.

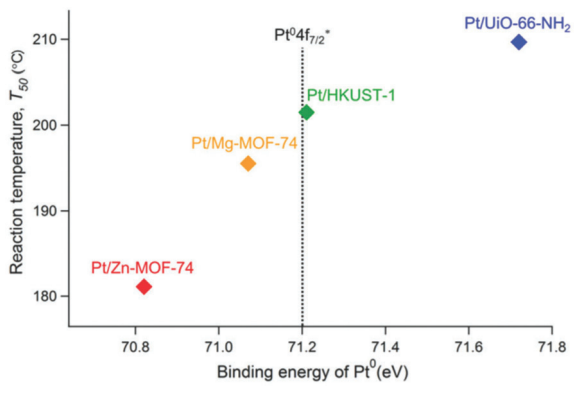

Fig. 9 Relationship between catalytic activity (*i.e.* reaction temperature, T_{50}) and electronic state of Pt NPs (*i.e.* binding energy of Pt^0 $4f_{7/2}$) of Pt/MOF catalysts. The black dotted line indicates the binding energy of bulk Pt^0 $4f_{7/2}$.

while almost no shifts in the other catalysts. The Zr 3d peaks in Cu/UiO-66-X shifted to lower binding energy compared to blank MOFs, suggesting the existence of the charge transfer from Cu NPs to the MOFs. Fig. 10 shows the relationship between catalytic activity for methanol production at 220 °C on the Cu catalysts and the binding energy shifts of the metal components in the supports. Cu/UiO-66-COOH and Cu/Hf-UiO-66 showed high catalytic activity for the methanol production, and the activity seems to be correlated with the order of the shift of the XPS peaks (*i.e.*, charge transfer), while the size of used Cu nanoparticles was not precisely the same (in range from 13 to 24 nm).

3.3 Substrate adsorption effect in M/MOFs

Selective adsorption for various guest molecules is one of the most important and specific properties of MOFs because of their well-defined porous structure and interactive inner surface, where the interaction with guest molecules is easily tuned by changing the inner component such as the functional group. Therefore, the M/MOFs should have a strong potential to enhance catalytic activity around the direct contact between metal NP and the MOF due to the strong adsorption of the specific substrate by the MOFs.

Yoshimaru *et al.* reported a systematic study of enhancement of the catalytic activity of metal NPs through the strong substrate adsorption by MOFs.[45] They demonstrated the catalytic activity for ethanol (EtOH) production through the acetic acid (AcOH) hydrogenation (AAH) reaction on Pt NPs supported on seven different MOFs, MIL-125-NH_2, UiO-66-NH_2, HKUST-1, MIL-101, Zn-MOF-74, Mg-MOF-74, and MIL-121, having a high tolerance for AcOH. In the AAH reaction, it is known that the ability of substrate adsorption by support material is a critical factor for high activity and that TiO_2 is the optimal support among traditional support materials.[23] The difference in the adsorption ability of MOFs for the AcOH substrate was demonstrated using temperature-programmed desorption-mass spectrometry (TPD-MS). TPD-MS charts of MIL-125-NH_2, UiO-66-NH_2, HKUST-1, and MIL-101 at a mass number (m/z) 60, corresponding to AcOH molecule, are shown in Fig. 11. No desorption peak was observed in other MOFs, showing their very weak adsorption strength for AcOH. The order of adsorption strength (*i.e.* desorption temperature) for AcOH is MIL-125-NH_2 > UiO-66-NH_2 > HKUST-1 > MIL-101 > other MOFs, suggesting that MOFs having an amino group tend to show a high affinity for the AcOH molecule due to the acid–base interaction.

The catalytic activity of Pt/MOF catalysts having a similar Pt diameter (~2 nm) and Pt loading amount (~0.5 wt%) is shown in Fig. 12. Pt/MIL-125-NH_2 and Pt/UiO-66-NH_2, in which the supports strongly adsorb AcOH, showed a high conversion of AcOH, reaching almost 100% above 260 °C, whereas Pt NPs on MOFs with a weak adsorption strength did not show an apparent catalytic activity. Considering the results of the adsorption

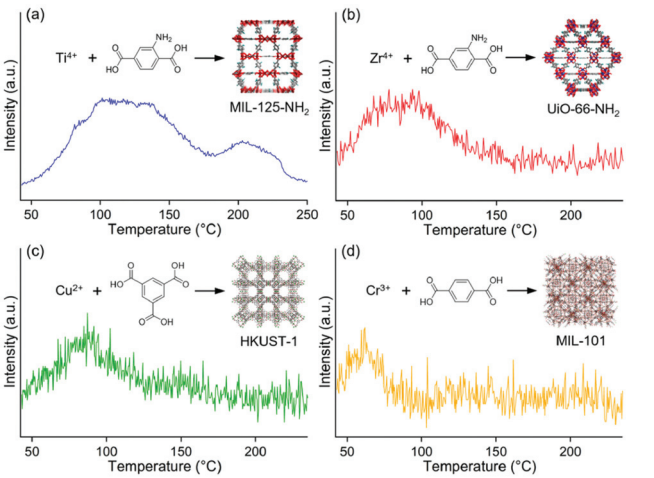

Fig. 11 TPD-MS charts of (a) MIL-125-NH_2, (b) UiO-66-NH_2, (c) HKUST-1, and (d) MIL-101 at m/z = 60 (for AcOH molecule). This figure has been reproduced from ref. 45 with permission from the American Chemical Society, copyright 2021.

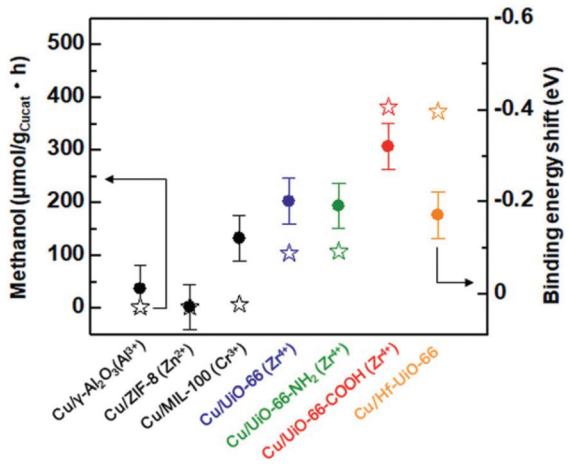

Fig. 10 Relationship between catalytic activity for methanol production and shift of binding energy of the metal component of support materials.

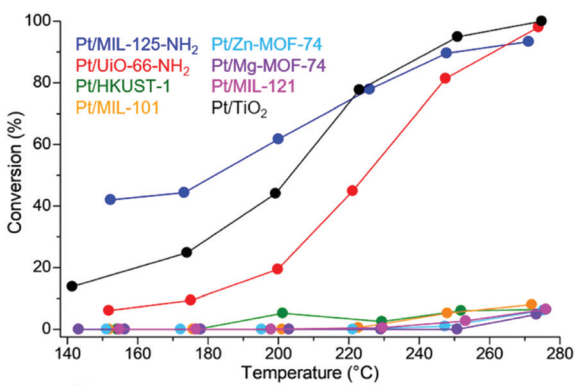

Fig. 12 Conversion of AcOH on Pt/MOFs and Pt/TiO_2. This figure has been reproduced from ref. 45 with permission from the American Chemical Society, copyright 2021.

strength for AcOH, this difference in catalytic activity clearly demonstrated a catalytic support effect regarding substrate adsorption of MOFs. Because the MOF supports (without Pt NPs) did not show catalytic activity, the active site was expected to be located around the interface between the Pt NP and the MOF or the area near the Pt NPs. The optimized traditional catalyst, Pt/TiO_2, also showed a high activity similar to $Pt/MIL\text{-}125\text{-}NH_2$ and $Pt/UiO\text{-}66\text{-}NH_2$. Importantly, the product selectivities of these catalysts ($Pt/MIL\text{-}125\text{-}NH_2$, $Pt/UiO\text{-}66\text{-}NH_2$, and Pt/TiO_2) were completely different (Fig. 13). The selectivity for the target product, EtOH, on $Pt/UiO\text{-}66\text{-}NH_2$ is immediately decreased with increasing reaction temperature, instead of increasing the ethyl acetate (AcOEt) by-product. Pt/TiO_2 showed a similar volcano-like curve of the selectivity for AcOEt with low selectivity for EtOH. By contrast, $Pt/MIL\text{-}125\text{-}NH_2$ selectively produced EtOH as the main product at almost all temperature regions and showed suppressed selectivity for AcOEt.

Fig. 14 shows the yield of EtOH, *i.e.* total performance for EtOH production, on the catalysts. Because of both high EtOH selectivity and activity, $Pt/MIL\text{-}125\text{-}NH_2$ showed the highest performance, which is apparently above the traditional optimal catalysts, Pt/TiO_2, in almost all temperature regions. The reason for high selectivity for EtOH or low selectivity for AcOEt was studied using infrared spectroscopy and a theoretical study (DFT calculation). The results revealed that the adsorption strength of $MIL\text{-}125\text{-}NH_2$ for EtOH is weaker than

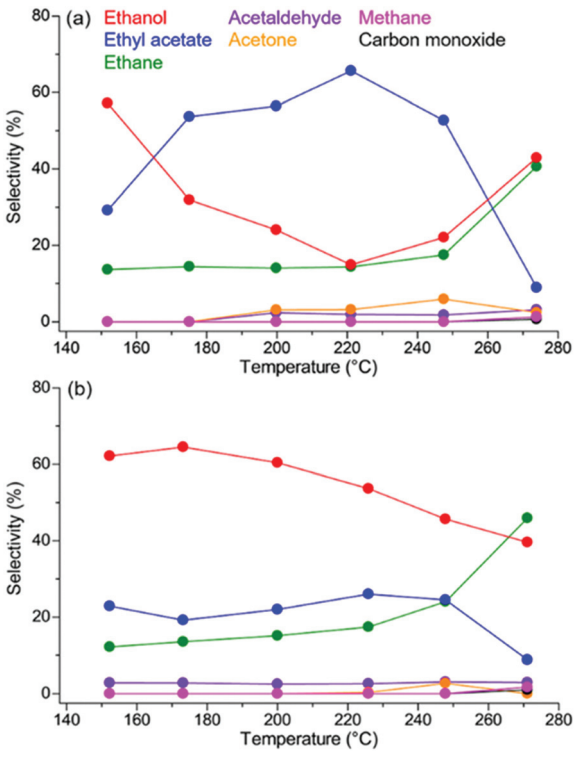

Fig. 13 Selectivity for each product on (a) $Pt/UiO\text{-}66\text{-}NH_2$ and (b) $Pt/MIL\text{-}125\text{-}NH_2$. This figure has been reproduced from ref. 45 with permission from the American Chemical Society, copyright 2021.

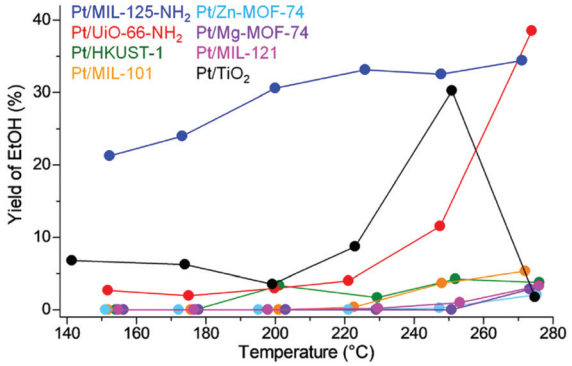

Fig. 14 EtOH yield on Pt/MOFs and Pt/TiO_2. This figure has been reproduced from ref. 45 with permission from the American Chemical Society, copyright 2021.

the other supports and thus the produced EtOH in $Pt/MIL\text{-}125\text{-}NH_2$ is immediately released outside the catalysts, which would suppress the formation of AcOEt from the produced EtOH and AcOH substrate. These results clearly indicated that MOF-based catalysts have a great potential to overcome the traditional oxide-based catalysts by using the support effects of MOFs regarding substrate adsorption.

Related to the guest adsorption, some researchers demonstrated that hydrophilicity or hydrophobicity of the MOF support is also an important factor for catalytic activity. Sun *et al.* reported a significant difference in catalytic activity for hydrodeoxygenation reaction of vanillin.[46] They revealed that Pd NPs supported on hydrophilic MOF, $MIL\text{-}101\text{-}SO_3Na$ ($Pd/MIL\text{-}101\text{-}SO_3Na$), showed higher catalytic performance for the reaction compared to that supported on hydrophobic supports of MIL-101 (Pd/MIL-101) and active carbon (Pd/C). The hydrophilic nature of the support allows the water soluble reactants to access the active sites easily and thus could enhance the catalytic activity. Another example was reported by Li *et al.*[47] They showed higher catalytic activity of $Pd@MIL\text{-}101\text{-}F_5$, having perfluoroalkyl groups, for dehydration coupling reaction of organosilane, compared to $Pd@MIL\text{-}101\text{-}NH_2$ and other Pd catalysts. The hydrophobic character of the $MIL\text{-}101\text{-}F_5$ contributes to construct well-accessible active sites. These examples clearly demonstrated that tuning of hydrophilicity or hydrophobicity of MOFs, *i.e.*, tuning of guest–MOF interaction, is an important way for creating highly active catalysts.

4. Conclusions and outlook

Three types of catalytic support effects, which were previously observed in traditional support materials, have recently been reported on MOF supports. The number of reports on the support effects of MOFs is still limited; however, there should be a strong potential in expanding it as one of the important research areas of both MOFs and heterogeneous catalysts. MOF-based catalysts could show higher catalytic performance (*i.e.* reactivity, selectivity, and yield for target product) than tra-

ditional catalysts by choosing optimal MOF supports having a limited pore size, various electronic states, and selective adsorption properties. Considering that the thermal stability of MOFs (<500 °C) is lower than that of conventional oxide supports, the reaction temperature of target catalysis should be carefully considered; the main research area of the MOF-based catalysts should be catalysis proceeding below 300 °C. The stability of MOFs against substrates should also be carefully considered for their application as supports. Recently, many researchers have investigated the chemical stability (*e.g.* against solvents, acid, or base) of MOFs and thus we could roughly estimate the applicability of MOFs for various substrates before catalytic application. Optimization of MOF supports for various catalyses would create new high-performance catalysts and provide attractive insights on the interaction between metallic NPs and MOFs.

Conflicts of interest

There are no conflicts to declare.

Acknowledgements

This work is partly supported by JSPS Grant-in-Aid for Scientific Research No. 17H04890.

References

1 Q. Qian, P. A. Asinger, M. J. Lee, G. Han, K. M. Rodriguesz, S. Lin, F. M. Benedetti, A. X. Wu, W. S. Chi and Z. P. Smith, *Chem. Rev.*, 2020, **120**, 8161–8266.
2 Y. Belmabkhout, P. M. Bhatt, K. Adil, R. S. Pillai, A. Cadiau, A. Shkurenko, G. Maurin, G. Liu, W. J. Koros and M. Eddaoudi, *Nat. Energy*, 2018, **3**, 1059–1066.
3 Y.-F. Zhang, Z.-H. Zhang, L. Ritter, H. Fang, Q. Wang, B. Space, Y.-B. Zhang, D.-X. Xue and J. Bai, *J. Am. Chem. Soc.*, 2021, **143**, 12202–12211.
4 D. E. Jaramillo, H. Z. H. Jiang, H. A. Evans, R. Chakraborty, H. Furukawa, C. M. Brown, M. H. Gordon and J. R. Long, *J. Am. Chem. Soc.*, 2021, **143**, 6248–6256.
5 H. D. Lawson, S. P. Walton and C. Chan, *ACS Appl. Mater. Interfaces*, 2021, **13**, 7004–7020.
6 K. Suresh and A. J. Matzger, *Angew. Chem., Int. Ed.*, 2019, **58**, 16790–16794.
7 Y. Yoshida, K. Kato and M. Sadakiyo, *J. Phys. Chem. C*, 2021, **125**, 21124–21130.
8 M. Sadakiyo and H. Kitagawa, *Dalton Trans.*, 2021, **50**, 5385–5397.
9 M. Sadakiyo, H. Kasai, K. Kato, M. Takata and M. Yamauchi, *J. Am. Chem. Soc.*, 2014, **136**, 1702–1705.
10 H. G. T. Nguyen, N. M. Schweitzer, C.-Y. Chang, T. L. Drake, M. C. So, P. C. Stair, O. K. Farha, J. T. Hupp and S. T. Nguyen, *ACS Catal.*, 2014, **4**, 2496–2500.
11 R.-J. Li, M. Li, X.-P. Zhou, D. Li and M. O'Keeffe, *Chem. Commun.*, 2014, **50**, 4047–4049.
12 W. Xie, Z. Gao, W.-P. Pan, D. Hunter, A. Singh and R. Vaia, *Chem. Mater.*, 2001, **13**, 2979–2990.
13 A. H. Jones, *J. Chem. Eng. Data*, 1960, **5**, 196–200.
14 M. Kandiah, M. H. Nilsen, S. Usseglio, S. Jakobsen, U. Olsbye, M. Tilset, C. Larabi, E. A. Quadrelli, F. Bonino and K. P. Lillerud, *Chem. Mater.*, 2010, **22**, 6632–6640.
15 W. Morris, C. J. Doonan, H. Furukawa, R. Banerjee and O. M. Yaghi, *J. Am. Chem. Soc.*, 2008, **130**, 12626–12627.
16 Y. Zhao, J. Zhang, J. Song, J. Li, J. Liu, T. Wu, P. Zhang and B. Han, *Green Chem.*, 2011, **13**, 2078–2082.
17 A. Aijaz, Q.-L. Zhu, N. Tsumori, T. Akita and Q. Xu, *Chem. Commun.*, 2015, **51**, 2577–2580.
18 M. Comotti, W.-C. Li, B. Spliethoff and F. Schüth, *J. Am. Chem. Soc.*, 2006, **128**, 917–924.
19 J. C. S. Wu, J. G. Goodwin and M. Davis, *J. Catal.*, 1990, **125**, 488–500.
20 A. Bruix, J. A. Rodriguez, P. J. Ramirez, S. D. Senanayake, J. Evans, J. B. Park, D. Stacchiola, P. Liu, J. Hrbek and F. Illas, *J. Am. Chem. Soc.*, 2012, **134**, 8968–8974.
21 H.-J. Freund and G. Pacchioni, *Chem. Soc. Rev.*, 2008, **37**, 2224–2242.
22 S. J. Tauster, S. C. Fung, R. T. K. Baker and J. A. Horsley, *Science*, 1981, **211**, 1121–1125.
23 W. Rachmady and M. A. Vannice, *J. Catal.*, 2000, **192**, 322–334.
24 M. M. Schubert, S. Hackenberg, A. C. Veen, M. Muhler, V. Plzak and R. J. Behm, *J. Catal.*, 2001, **197**, 113–122.
25 M. Kitano, Y. Inoue, Y. Yamazaki, F. Hayashi, S. Kanbara, S. Matsuishi, T. Yokoyama, S. W. Kim, M. Hara and H. Hosono, *Nat. Chem.*, 2012, **4**, 934–940.
26 T.-N. Ye, S.-W. Park, Y. Lu, J. Li, M. Sasase, M. Kitano and H. Hosono, *J. Am. Chem. Soc.*, 2020, **142**, 14374–14383.
27 D. Deng, K. S. Novoselov, Q. Fu, N. Zheng, Z. Tian and X. Bao, *Nat. Nanotechnol.*, 2016, **11**, 218–230.
28 Y. K. Hwang, D.-Y. Hong, J.-S. Chang, S. H. Jhung, Y.-K. Seo, J. Kim, A. Vimont, M. Daturi, C. Serre and G. Férey, *Angew. Chem., Int. Ed.*, 2008, **47**, 4144–4148.
29 Q.-L. Xhu, J. Li and Q. Xu, *J. Am. Chem. Soc.*, 2013, **135**, 10210–10213.
30 S. Hermes, M.-K. Schröter, R. Schmid, L. Khodeir, M. Muhler, A. Tissler, R. W. Fischer and R. A. Fischer, *Angew. Chem., Int. Ed.*, 2005, **44**, 6237–6241.
31 J. Hermannsdörfer, M. Friedrich, N. Miyajima, R. Q. Albuquerque, S. Kümmel and R. Kempe, *Angew. Chem., Int. Ed.*, 2012, **51**, 11473–11477.
32 T. Ishida, M. Nagaoka, T. Akita and M. Haruta, *Chem. – Eur. J.*, 2008, **14**, 8456–8460.
33 H.-L. Jiang, B. Liu, T. Akita, M. Haruta, H. Sakurai and Q. Xu, *J. Am. Chem. Soc.*, 2009, **131**, 11302–11303.
34 G. Lu, S. Li, Z. Guo, O. K. Farha, B. G. Hauser, X. Qi, Y. Wang, X. Wang, S. Han, X. Liu, J. S. DuChene, H. Zhang, Q. Zhang, X. Chen, J. Ma, S. C. J. Loo, W. D. Wei, Y. Yang and J. T. Hupp, *Nat. Chem.*, 2012, **4**, 310–316.

35 J. Zhou, P. Wang, C. Wang, Y. T. Goh, Z. Fang, P. B. Messersmith and H. Duan, *ACS Nano*, 2015, **9**, 6951–6960.
36 M. Mukoyoshi, H. Kobayashi, K. Kusada, M. Hayashi, T. Yamada, M. Maesato, J. M. Taylor, Y. Kubota, K. Kato, M. Takata, T. Yamamoto, S. Matsumura and H. Kitagawa, *Chem. Commun.*, 2015, **51**, 12463–12466.
37 M. Sadakiyo, S. Yoshimaru, H. Kasai, K. Kato, M. Takata and M. Yamauchi, *Chem. Commun.*, 2016, **52**, 8385–8388.
38 P. Wang, J. Zhao, X. Li, Y. Yang, Q. Yang and C. Li, *Chem. Commun.*, 2013, **49**, 3330–3332.
39 Z. Guo, C. Xiao, R. V. Maligal-Ganesh, L. Zhou, T. W. Goh, X. Li, D. Tesfagaber, A. Thiel and W. Huang, *ACS Catal.*, 2014, **4**, 1340–1348.
40 J. Zhou, P. Wang, C. Wang, Y. T. Goh, Z. Fang, P. B. Messersmith and H. Duan, *ACS Nano*, 2015, **9**, 6951–6960.
41 X. Li, T. W. Goh, L. Li, C. Xiao, Z. Guo, X. C. Zeng and W. Huang, *ACS Catal.*, 2016, **6**, 3461–3468.
42 S. Yoshimaru, M. Sadakiyo, A. Staykov, K. Kato and M. Yamauchi, *Chem. Commun.*, 2017, **53**, 6720–6723.
43 Y. P. G. Chua, G. T. K. K. Gunasooriya, M. Saeys and E. G. Seebauer, *J. Catal.*, 2014, **311**, 306–313.
44 H. Kobayashi, J. M. Taylor, Y. Mitsuka, N. Ogiwara, T. Yamamoto, T. Toriyama, S. Matsumura and H. Kitagawa, *Chem. Sci.*, 2019, **10**, 3289–3294.
45 S. Yoshimaru, M. Sadakiyo, N. Maeda, M. Yamauchi, K. Kato, J. Pirillo and Y. Hijikata, *ACS Appl. Mater. Interfaces*, 2021, **13**, 19992–20001.
46 Q. Sun, M. Chen, B. Aguila, N. Nguyen and S. Ma, *Faraday Discuss.*, 2017, **201**, 317–326.
47 L. Li, Z. Li, W. Yang, Y. Huang, G. Huang, Q. Guan, Y. Dong, J. Lu, S.-H. Yu and H.-L. Jiang, *Chem*, 2021, **7**, 686–698.